Side chain engineering in indacenodithiophene-*co*-benzothiadiazole and its impact on mixed ionic-electronic transport properties

Isabelle Holzer,[1,†] Vincent Lemaur,[2,†] Meng Wang,[3,4,†] Han-Yan Wu,[5,†] Lu Zhang,[6] Raymundo Marcial-Hernandez,[3] Peter Gilhooly-Finn,[3] Priscila Cavassin,[1] Sébastien Hoyas,[2,7] Dilara Meli,[8] Ruiheng Wu,[9] Bryan D. Paulsen,[10] Joseph Strzalka,[11] Andrea Liscio,[12] Jonathan Rivnay,[10,13] Henning Sirringhaus,[6] Natalie Banerji,[1,*] David Beljonne,[2,*] Simone Fabiano,[5,*] and Christian B. Nielsen[3,*]

[1]Department of Chemistry, Biochemistry and Pharmaceutical Sciences (DCBP), University of Bern, Freiestrasse 3, 3012 Bern, Switzerland. E-mail: natalie.banerji@unibe.ch

[2]Laboratory for the Chemistry of Novel Materials, Materials Research Institute, University of Mons, Place du Parc 20, Mons, BE-7000, Belgium. E-mail: david.beljonne@umons.ac.be

[3]Department of Chemistry, Queen Mary University of London, Mile End Road, London E1 4NS, UK. E-mail: c.b.nielsen@qmul.ac.uk

[4]i-Lab & Printable Electronics Research Center, Suzhou Institute of Nano-Tech and Nano-Bionics, Chinese Academy of Sciences, 398 Ruoshui Road, SEID, SIP, Suzhou, 215123, P. R. China

[5]Laboratory of Organic Electronics, Department of Science and Technology, Linköping University, SE-601 74 Norrköping, Sweden. E-mail: simone.fabiano@liu.se

[6]Optoelectronics Group, Cavendish Laboratory, JJ Thomson Avenue, Cambridge CB3 0HE, UK.

[7]Organic Synthesis & Mass Spectrometry Laboratory, Interdisciplinary Center for Mass Spectrometry (CISMa), Center of Innovation and Research in Materials and Polymers (CIRMAP), University of Mons - UMONS, 23 Place du Parc, 7000 Mons, Belgium

[8]Department of Materials Science and Engineering, Northwestern University, Evanston, Illinois 60208, USA.

[9]Department of Chemistry, Northwestern University, Evanston, Illinois 60208, USA.

[10]Department of Biomedical Engineering, Northwestern University, Evanston, Illinois 60208, USA.

[11]X-Ray Science Division, Argonne National Laboratory, Lemont, Illinois 60439, USA.

[12]Istituto per la Microelettronica e Microsistemi, CNR, Roma Unit, via del fosso del cavaliere 100, 00133 Roma, Italy.

[13]Simpson Querrey Institute, Northwestern University, Chicago, Illinois 60611, USA.

[†]These authors contributed equally.

Abstract

Organic semiconductors are increasingly being decorated with hydrophilic solubilising chains to create materials that can function as mixed ionic-electronic conductors, which are promising candidates for interfacing biological systems with organic electronics. While numerous organic semiconductors, including p- and n-type materials, small molecules and polymers, have been successfully tailored to encompass mixed conduction properties, common to all these systems is that they have been semicrystalline materials. Here, we explore how side chain engineering in the nano-crystalline indacenodithiophene-*co*-benzothiadiazole (IDTBT) polymer can be used to instil ionic transport properties and how this in turn influences the electronic transport properties. This allows us to ultimately assess the mixed ionic-electronic transport properties of these new IDTBT polymers using the organic electrochemical transistor as the testing platform. Using a complementary experimental and computational approach, we find that polar IDTBT derivatives can be infiltrated by water and solvated ions, they can be electrochemically doped efficiently in aqueous electrolyte with fast doping kinetics, and upon aqueous swelling there is no deterioration of the close interchain contacts that are vital for efficient charge transport in the IDTBT system. Despite these promising attributes, mixed ionic-electronic charge transport properties are surprisingly poor in all the polar IDTBT derivatives. Albeit a "negative" result, this finding clearly contradicts established side chain engineering rules for mixed ionic-electronic conductors, which motivated our continued investigation of this system. We eventually find this anomalous behaviour to be caused by increasing energetic disorder in the polymers with increasing polar side chain content. We have investigated computationally how the polar side chain motifs contribute to this detrimental energetic inhomogeneity and ultimately use the learnings to propose new molecular design criteria for side chains that can facilitate ion transport without impeding electronic transport.

Introduction

A rapidly growing interest in the field of organic bioelectronics with emerging applications such as bioelectronic sensors and neuromorphic devices has spurred significant attention to the concept of mixed ionic and electronic conduction that merges the language of biology (ionic charges) with that of electronics (electronic charges).[1–3] Engineering of organic mixed ionic-electronic conductors (OMIECs) can be approached through rational materials choice, for instance by mixing an electrically conducting polymer with an ionomer as seen in the case of poly(3,4-ethylenedioxythiophene):polystyrene sulfonate.[4–6] Chemical engineering offers another approach whereby organic semiconductors can be structurally modified, typically with hydrophilic or ionic moieties, to afford mixed ionic-electronic properties within a single active material.[7–10] While both approaches have their advantages and disadvantages, a greater selection of OMIECs with varied properties is needed to facilitate the continued growth of organic bioelectronics.

Taking advantage of the vast knowledge generated during the last few decades of organic electronics research, many high-performing organic charge-transport materials have successfully been chemically modified to encompass mixed ionic-electronic transport properties. This includes for instance hole-transporting (p-type) thiophene-based small-molecule and polymeric semiconductors as well as electron-transporting (n-type) rylene diimide-based materials chemically modified with e.g., oligoether chains, hydroxyl- or sulfonate-terminated alkyl chains.[8–12] Donor-acceptor-type structures, benefiting from strong intramolecular interactions between alternating electron-rich and -deficient units to modulate the frontier energy levels, have likewise been synthetically modified to ensure ionic transport in the bulk semiconductor film as exemplified by recent studies of diketopyrrolopyrrole- and isoindigo-based polymers functionalised with oligoether side chains.[13–17] A common theme emerging from these studies across different classes of organic semiconductors is that a good electronic charge transport material can be turned into a good mixed ionic-electronic charge transport material simply by replacing the non-polar solubilising substituents with polar alternatives. Among the plethora of donor-acceptor materials from the organic electronics literature,

the indacenodithiophene-*co*-benzothiadiazole (IDTBT) polymer has often been highlighted due to a reliably high hole mobility above 1 cm^2/Vs with near-ideal field-effect transistor characteristics despite a lack of long-range crystalline order.[18,19,20] The highly efficient charge transport in the solid state is attributed to a torsion-resilient backbone conformation leading to a low degree of energetic disorder and fast intrachain charge transport with only a few interchain contacts needed for efficient long-range transport.[21] As such, IDTBT appears as a promising polymer backbone for OMIECs materials development and an obvious platform for side chain engineering studies.

With these considerations in mind, we have systematically substituted fractions of the usual *n*-hexadecyl (C16) solubilising side chains of IDTBT-C16 with more polar ethylene glycol-containing side chains to study the impact on ionic and electronic charge transport properties. More precisely, the introduced amphipathic side chains comprise an initial non-polar five-carbon spacer unit separating the polymer backbone from a polar methyl-terminated triethylene glycol unit to keep the side chain length identical to the original C16 chain. Employing a statistical (random) copolymerisation protocol, 10%, 50% and 100% of the C16-bearing indacenodithiophene units have been substituted for the corresponding indacenodithiophene motifs with amphipathic side chains. Undertaking a joint experimental and computational approach, we have subsequently studied in detail how the resulting polymers interact with solvated ions, how they conduct electronic charges and how they respond to electrochemical and chemical doping. To our surprise, we have found that IDTBT *does not* conform to the established side chain engineering rules; it *does not* readily function as a mixed ionic-electronic conductor upon the introduction of polar oligoether side chains. Finally, we have used the accumulated understanding of this system to refine our current comprehension of side chain engineering and propose new side chain design criteria for optimising mixed ionic-electronic conduction properties in near-amorphous semiconducting polymers.

Results and discussion

Polymer synthesis and characterisation

The IDTBT copolymer series presented in Figure 1a, comprising different ratios of the glycolated IDT monomer containing 2,5,8,11-tetraoxahexadecane side chains and the commonly used hexadecyl substituted IDT monomer, was synthesised via Suzuki-Miyaura polymerisation by adapting the reported literature procedure.[18] The well-known IDTBT-C16 (denoted IDTBT-P0 herein) was synthesised as a reference material to thereafter proceed with co-polymerisations using 10%, 50% and 100% loading of the polar IDT monomer to afford polymers IDTBT-P10, IDTBT-P50 and IDTBT-P100.[22] Detailed conditions of monomer and polymer synthesis are described in the Supporting Information. ^{1}H NMR analysis (Figure 1b and SI Section 1) confirmed that the ratios between glycolated and alkylated IDT moieties in the mixed copolymers were close to the expected based on monomer feed ratios; polar content of 11 % and 51 %, respectively, was found for IDTBT-P10 and IDTBT-P50. The number average molecular weight (M_n) and dispersities (PDI) of the polymers were determined by gel permeation chromatography. Non-polar IDTBT-P0 displayed the highest molecular weight (M_n = 58 kDa, PDI = 1.2), meanwhile IDTBT-P10 (M_n = 48 kDa, PDI = 1.2) and IDTBT-P50 (M_n = 48 kDa, PDI = 1.3) presented comparable values, however IDTBT-P100 (M_n = 18 kDa, PDI = 1.8) showed a considerably lower degree of polymerisation indicating that the 100% loading of the polar IDT monomer negatively affected the chain growth of the polymer.

UV-vis absorption spectroscopy of polymer thin films spin-cast from *o*-dichlorobenzene (ODCB) onto glass substrates is presented in Figure 1c. It can be observed that IDTBT-P10 and IDTBT-P50 share a maximum absorption peak with IDTBT-P0 at 678 nm, with a slight increase in the shoulder at 624 nm with increasing polar content. The main absorption feature of IDTBT-P100 is blue-shifted by 14 nm relative to the other polymers with a slightly broader shape; this might be attributed to the somewhat lower degree of polymerisation and a more disordered morphology. The higher energy absorption feature observed for all the polymers around 400 nm is attributed to the π-π^* transitions.

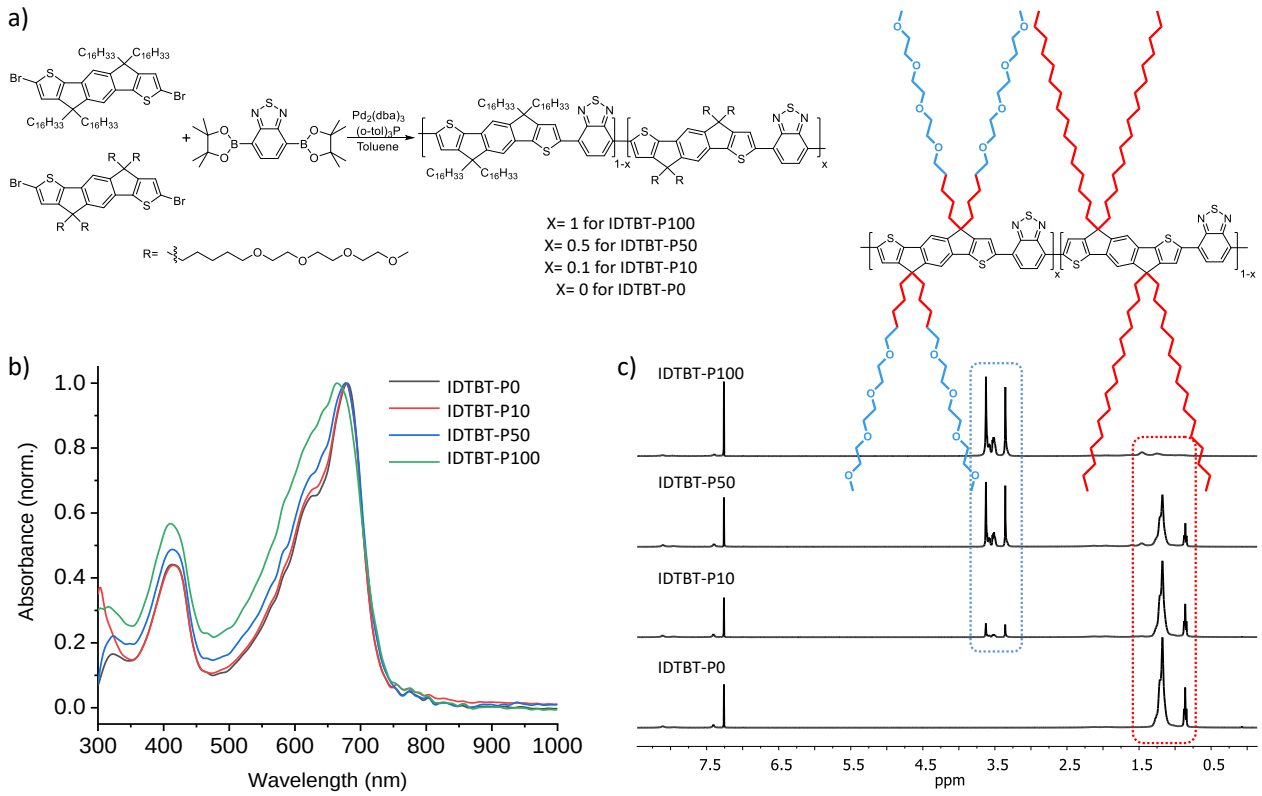

Figure 1*: a) Synthetic scheme outlining the IDTBT polymer synthesis employing different ratios of the polar and nonpolar IDT monomers. b) UV-vis spectra of thin polymer films obtained by spin-coating from 10 mg/ml ODCB solutions at 80°C; 2000 rpm for 90 s then 8000 rpm for 30 s. Dried in vacuum oven at 40°C for 30 mins. c)* ^{1}*H NMR spectra of the IDTBT polymers highlighting the peaks from polar (blue box) and nonpolar (red box) side chain moieties.*

Contact angle measurements were performed to better understand the polarity and wettability of the polymer thin film surfaces. IDTBT-P0 presented a contact angle of 85°±0.3 with water and the introduction of 10% of the polar monomer led to a lower contact angle (74°±0.2), this effect is stronger with 50% incorporation of the polar monomer (61°±0.6), but no further decrement of the contact angle is observed for the fully glycolated polymer (IDTBT-P100, 63°±0.3, Figure S1). The polymers thus showed increased hydrophilicity and wettability with increasing polar content with a limit close to 60° in contact angle with water.

The surface work function of each polymer was investigated using the Kelvin probe technique. Thin films were spin-cast from ODCB solutions onto silicon substrates. It was found that the surface work function of the polymer films decreased with increasing polar content. IDTBT-P0, P10, P50 and P100 afforded work functions of 4.98 eV, 4.95 eV, 4.88 eV, and 4.70 eV, respectively (Figure S2). Although the work function depends on several factors like the orientation of the polymer near the surface, the exposure to ambient conditions and residual solvent, the trend reflects the increasing content of electron-donating oligoether chains when going from IDTBT-P0 to IDTBT-P100. The work function values are moreover close to that reported for polycrystalline gold under ambient conditions (~5.1 eV),[23] which could potentially lead to low contact resistance when using gold contacts in electrical measurements.[24]

Cyclic voltammetry measurements on polymer thin films spin-cast from ODCB were conducted with tetrabutylammonium hexafluorophosphate electrolyte in acetonitrile at various scan rates (see Figure S3). The onset of oxidation was found to decrease with increasing polar content in agreement with the Kelvin probe data reflecting the more facile ion penetration into the polymer films with increasing polar content.

Grazing incidence wide-angle X-ray scattering (GIWAXS) was performed to investigate the structural properties of the polymer thin films (Figure 2 and Figure S4). A predominant face-on orientation of the polymer backbone relative to the substrate is observed; fittings of the in-plane peaks at low q-values and the out-of-plane peaks at higher q-values afford along-chain repeat distances in the range 15.5 – 15.7 Å and π-stacking distances from 4.15 to 4.35 Å across the polymer series. IDTBT-P100 is significantly more amorphous than the other three IDTBT polymers who show similar along-chain coherence lengths in the range 97 – 114 Å and a slight decrease of the second order (002) along-chain peak when going from IDTBT-P0 to IDTBT-P10 and IDTBT-P50; IDTBT-P100, on the other hand, shows no discernible (00l) along-chain peaks in the in-plane direction. Longer π-stacking distances (4.34 – 4.35 Å) for IDTBT-P10 and IDTBT-P50 than for IDTBT-P0 and IDTBT-P100 (4.29 Å and 4.15 Å, respectively) suggest that the mixed copolymer design with polar

and non-polar side chains randomly distributed along the polymer backbone leads to less favourable polymer backbone interactions than seen for the two polymers decorated entirely with polar or non-polar side chains.

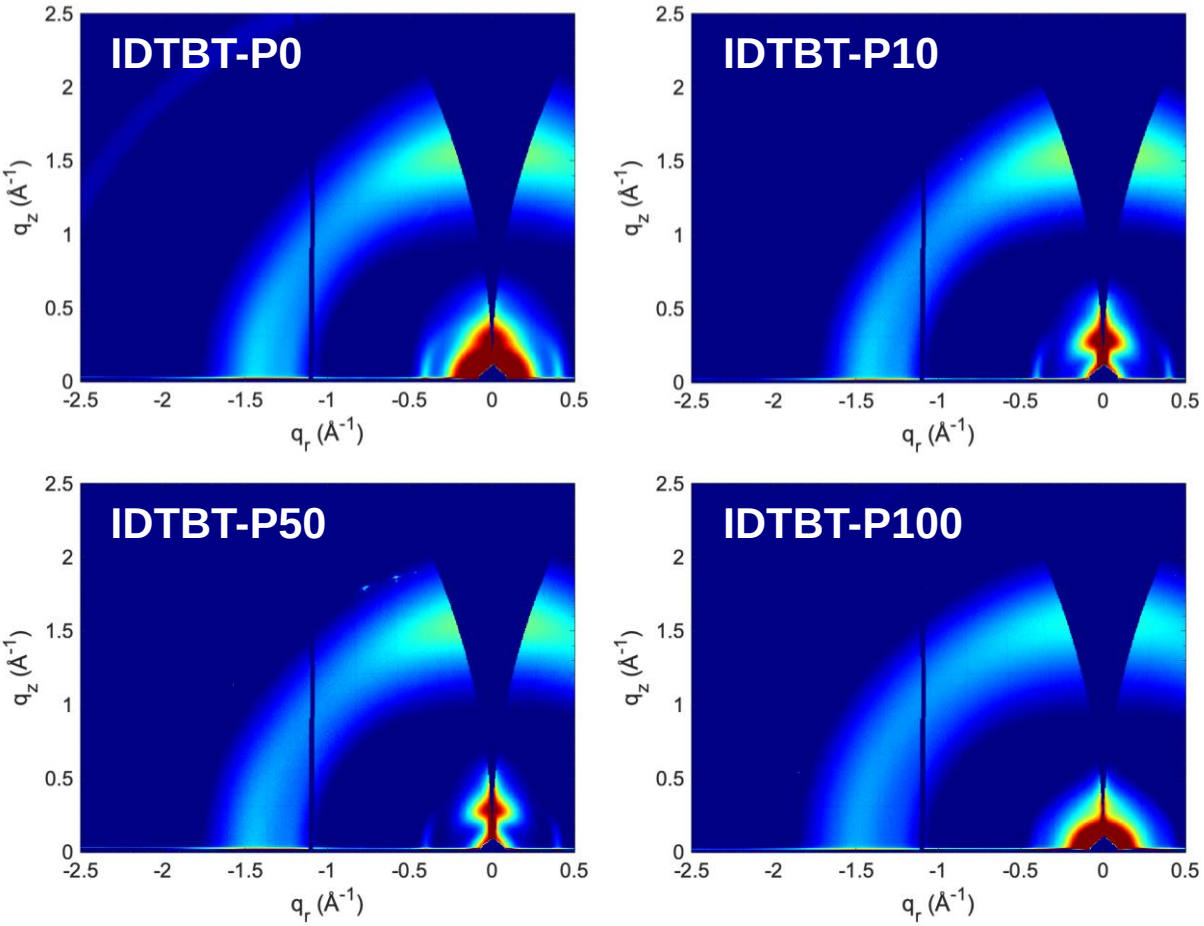

***Figure 2**: 2D GIWAXS scattering patterns for the IDTBT polymer series.*

Mixed ionic-electronic transport properties

Following the characterisation of the IDTBT copolymers, we investigated the mixed ionic-electronic transport properties to validate our molecular design strategy. To this end, the organic electrochemical transistor (OECT) is an ideal platform due to the three-electrode configuration with electrochemical gating facilitated by an electrolyte solution directly in contact with the active layer. This allows for ions to infiltrate the semiconductor film and compensate the electronic charges that can be injected into (or extracted from) the bulk semiconductor layer via the source and drain electrodes. The OECT performance of the four polymers was evaluated using both aqueous and non-aqueous electrolytes. For the aqueous system, OECTs were measured with a 0.1 M NaCl electrolyte,

however, none of the four IDTBT polymers showed typical output and transfer characteristics when biased between 0 and -0.7 V (Figure 3 and Figure S5). To explore a larger electrochemical window, non-aqueous OECTs were tested with 0.1 M LiOTf and 0.1 M $NaClO_4$ in acetonitrile and biased up to -2.0 V during the gate sweep (Figure 3c,g and Figure S6). To mimic the conditions where we see efficient electrochemical doping (*vide infra*), non-aqueous OECTs were also tested with 0.1 M $TBAPF_6$ in acetonitrile (Figure S9). Finally, OECTs were tested with the ionic liquid 1-ethyl-3-methylimidazolium bis(trifluoromethylsulfonyl)imide ([EMIM][TFSI], Figure S7 and S8). None of the polymers showed typical output and transfer characteristics when tested in acetonitrile irrespective of choice of electrolyte. Only with the [EMIM][TFSI] ionic liquid electrolyte, small current responses (<1 µA) were observed for IDTBT-P10 and IDTBT-P50 (Figure 3d,h) although meaningful figures-of-merit could not be extracted. These surprising results on the mixed ionic-electronic transport led us to interrogate in greater detail both the ionic transport and the electronic transport properties to elucidate the underlying reasons for the lack of efficient mixed transport in this polymer system.

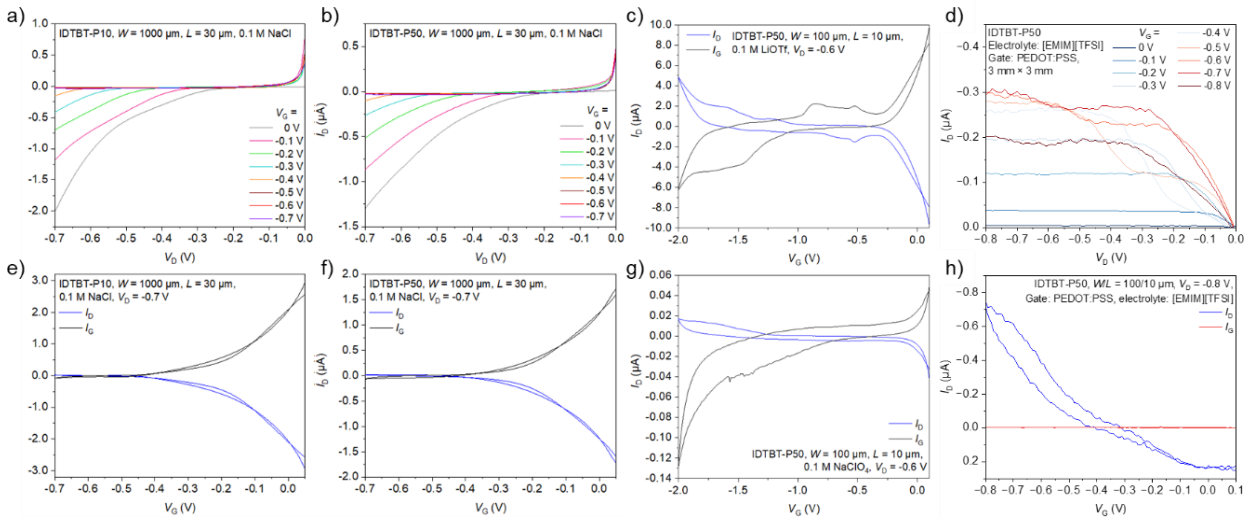

Figure 3*: Electrical performance of IDTBT-P10 and IDTBT-P50-based OECTs; (a-b) output curves and (e-f) transfer curves for IDTBT-P10 and IDTBT-P50-based devices in 0.1 M NaCl aqueous electrolyte; (c,g) transfer curves for IDTBT-P50-based devices in 0.1 M LiOTf and 0.1 M* $NaClO_4$

acetonitrile electrolytes; (d,h) output and transfer curves for IDTBT-P50-based devices in ionic liquid electrolyte with PEDOT:PSS as the gate.

Ionic transport and electrochemical doping

An electrochemical quartz crystal microbalance (eQCM) was used to investigate the static swelling properties of the four polymers in water. IDTBT-P0, IDTBT-P10, IDTBT-P50, and IDTBT-P100 swell 0%, 2%, 9% and 12% respectively (Table S1 and Figure S10). Without the polar side chains, the IDTBT-P0 thin film does not absorb any aqueous electrolyte within the detection limit of the eQCM technique. As the polar side chain content increases, the degree of swelling grows gradually up to 12% for IDTBT-P100. This trend indicates that the introduction of glycolated side chains enhances the hydrophilicity of the IDTBT polymers, which is consistent with the molecular design and the contact angle and cyclic voltammetry data discussed above.

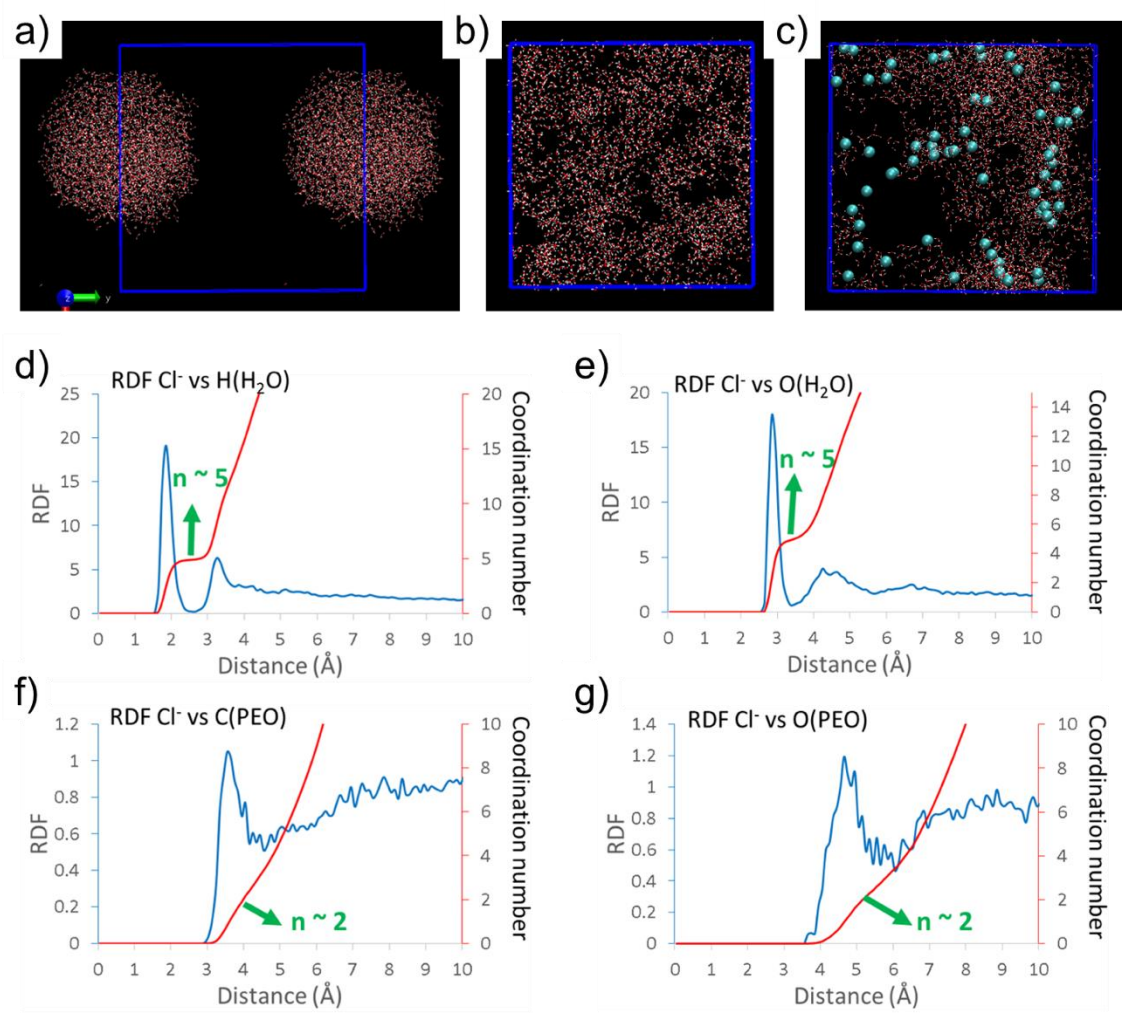

Figure 4*: Representation of the simulated distributions of water molecules in amorphous phases of IDTBT-P0 + 25%wt of water (a) and IDTBT-P100 + 25% of water (b) after a 2ns-long molecular dynamics (NPT, p = 1 atm, T = RT). Representation of the simulated distribution of the water molecules and chlorine anions (cyan balls) in an amorphous phase of charged IDTBT-P100 + 25%wt of water + 60 chlorine anions after a 2ns-long molecular dynamics (NPT, p = 1 atm, T = RT) (c). The polymer chains have been omitted for clarity. Radial distribution functions (blue) and coordination numbers (red) between the chlorine anions and the hydrogen atoms of the water molecules (d); the oxygen atoms of the water molecules (e); the carbon atoms of the polar side chains (f); and the oxygen atoms of the polar side chains (g); as calculated from the analysis of the 10 snapshots of the MD trajectory for the system containing 20 charged hexamers of IDTBT, 25%wt of water and 60 chlorine anions.*

The dispersion of water molecules (and associated ions) was further investigated from a computational perspective using classical force-field molecular mechanics (MM) and molecular dynamics (MD) simulations focusing on the extreme cases of IDTBT-P0 and IDTBT-P100. To proceed with this, we first benchmarked our force field by constructing the most stable supramolecular organizations of *dry* IDTBT-P0[25] and IDTBT-P100 films (see SI section 8). Stable crystal arrangements for both polymers (Figure S11) correspond to a cofacial arrangement of two inequivalent polymer chains. In both cases, the side chains are interdigitated between the successive layers of π-stacked chains. Lattice parameters compare favourably with experimental data available from earlier investigations for IDTBT-P0 and with the results of the GIWAXS measurements reported here.[21,26] The impact on the resulting morphology of the presence of water molecules inside the IDTBT co-polymer amorphous films was subsequently estimated by mixing 20 hexamers of IDTBT-P0 or IDTBT-P100 with 5%wt (442 molecules) and 25%wt (2210 molecules) of water. We obtained very different results for IDTBT-P0 versus IDTBT-P100. In the case of the P0 polymer chains, carrying apolar side chains, all water molecules aggregate as bubbles when inserted into the films, while the water molecules get fully dispersed during the MD simulations of the P100 films (see Figure

4a-b). At this point, and very much in line with chemical intuition, we can thus deliberately disregard P0 as a possible candidate for OECT applications, because of the very poor uptake of water.

To mimic the working principle of an OECT, a system made of 20 hexamers of IDTBT-P100, 25%wt of water and 60 chlorine anions was studied next. Here, to ensure the electroneutrality of the system, 60 positive charges have been added uniformly on the conjugated atoms of P100. The morphology of this system is represented in Figure 4c and reveals that: (i) the water molecules are still reasonably well dispersed throughout the films, though not as uniformly as in the water-only case; and (ii) that the chlorine atoms are preferentially located in water-rich regions. To analyse the relative position of the chlorine atoms in the film, radial distribution functions (RDF) and coordination numbers have been calculated on the 10 snapshots of the MD trajectory (Figure 4d-g). Not surprisingly, the RDF curves suggest a strong interaction between the chlorine ions and the water molecules (mostly with the hydrogen atoms). With a coordination number of five, our RDF analysis suggests that chlorine anions are, on average, solvated by five water molecules (Figure 4d-e). Chlorine atoms are also interacting with the polar side chains since the calculated coordination numbers between the chlorine anions and either the carbons or oxygens of the polar side chains is two (Figure 4f-g). Chlorine anions are in contrast less likely to interact with the conjugated backbones, the coordination numbers being small for all conjugated atoms (see Table S2). This should also have a positive impact on charge transport, as trapping of the majority hole carriers by chlorine anions should be limited.

With confirmation that water molecules (and associated ions) can infiltrate the polar IDTBT derivatives, we next turned our attention to the electrochemical doping process using *in-situ* time-resolved Vis-NIR spectroelectrochemistry. Spectroelectrochemical experiments were carried out, using 0.1 M $TBAPF_6$ in acetonitrile as electrolyte and an Ag/AgCl counter electrode and thin films of ~25 and ~200 nm deposited via spin coating onto ITO substrates. A home-built setup was used, where polychromatic light is transmitted through the sample and simultaneously detected with two spectrophotometers in the visible and near-infrared range. Square pulses of voltage ranging from -0.1

to -1.3 V with 0.1 V steps were applied for 5 s. Each doping step was followed by a subsequent dedoping step for 5 s at 0 V. In Figure 5a, the absorbance spectra for different voltages of IDTBT-P50 (28 nm) are displayed. The spectra for the other IDTBT polymers are included in the Supplementary Information (Figure S13). From -0.1 to -0.8 V, one main band at around 670 nm is present, which is ascribed to the absorption of the neutral polymer. At higher doping voltages, a second band at around 1020 nm and a third band at around 1450 nm appear. Those are attributed to polarons and bipolarons, respectively.[26,27]

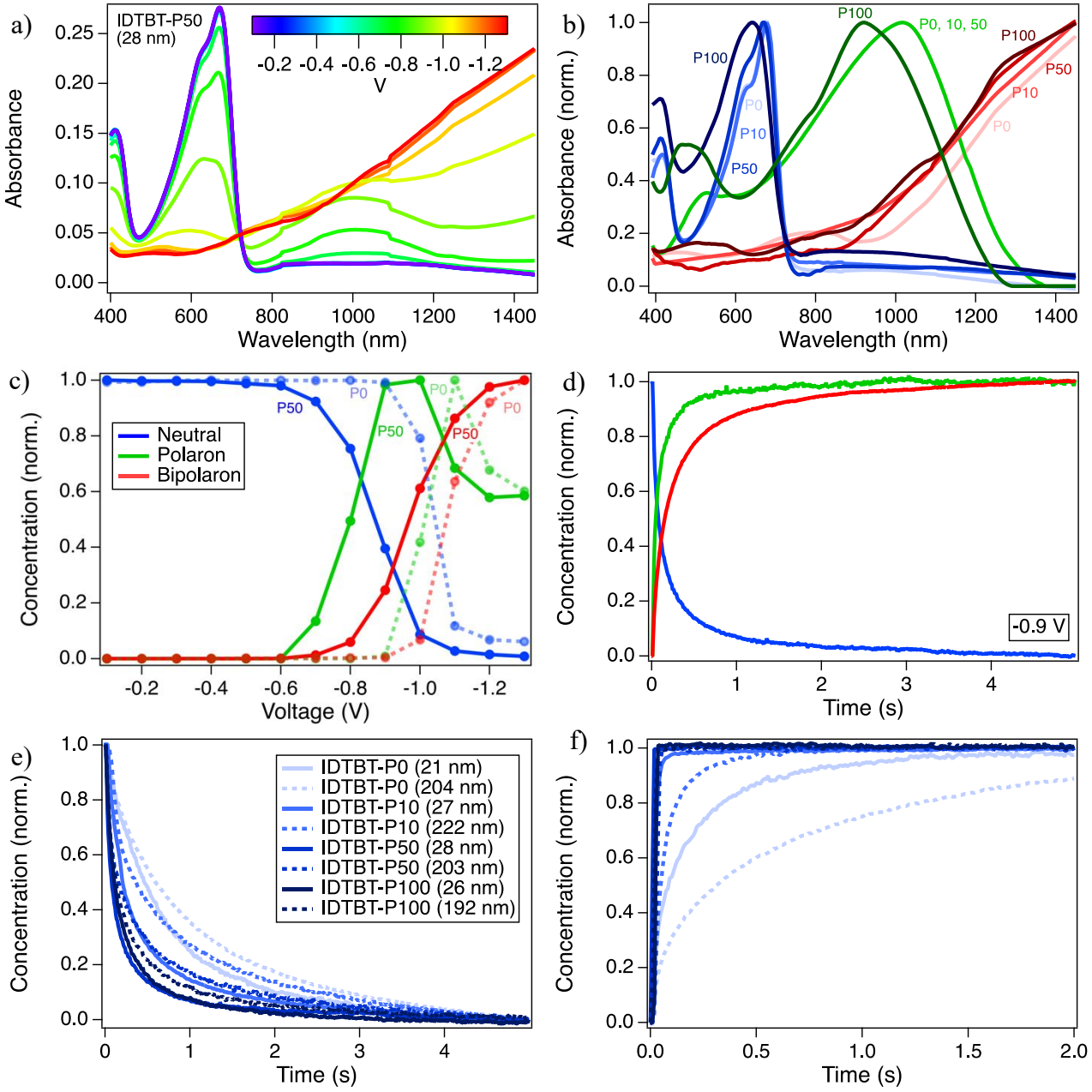

***Figure 5**: a) Absorption spectra of IDTBT-P50 (28 nm) upon application of doping voltage ranging from -0.1 V to -1.3 V (ΔV = -0.1 V) versus Ag/AgCl. b) Spectral signature of each species obtained from the MCR analysis in the different films and c) their corresponding normalized concentration for IDTBT-P50 (solid lines) and IDTBT-P0 (dashed lines) as a function of voltage. d) Time-resolved normalized species concentration for the doping at -0.9 V of IDTBT-P50. e) Comparison of the doping dynamics at lower doping level for the neutral species in the different thick and thin films, and f) comparison of the corresponding dedoping dynamics.*

To decompose the absorption spectra into the different species and their respective concentrations, we used Multivariate Curve Resolution (MCR) analysis. The spectral components for the ~25 nm thick films are shown in Figure 5b (Figure S14 for all films). The shape of the neutral polymer absorbance around 670 nm was adapted to account for the spectral changes between the materials shown in Figure 1b) (notably, IDTBT-P100 has a broader and more unstructured signature). The polaron component centred around 1020 nm is also broader for IDTBT-P100, while a similar spectrum could be used for the other films, and a comparable bipolaron component around 1450 nm was found in all cases. From the MCR analysis, the evolution of the species as a function of voltage is extracted and compared for IDTBT-P50 (28 nm) and IDTBT-P0 (21 nm) in Figure 5c). The plots of the other polymers are included in Figures S15 and S16. In agreement with the cyclic voltammetry and Kelvin probe data, the onset of the oxidation of the neutral species to polarons decreases from about -0.8 V to -0.6 V with increasing polar content, and the formation of bipolarons shifts from -0.9 V to -0.8 V. The neutral species are depleted until -1.1 V in all films and the polaron concentration decreases at high oxidation voltages, as polarons are converted to a rising population of bipolarons. We also recorded the current of the devices by chronoamperometry and deduced the injected or extracted charge carrier density during the doping and dedoping processes (Figures S17 and S18). The onsets and trends with voltage closely follow the spectroelectrochemical changes in the different materials.

The dynamics of the doping processes in the IDTBT polymers was investigated using time-resolved spectroelectrochemistry with a resolution of 10 ms. The MCR components from the steady-state spectra were used to obtain the temporal evolution of the neutral, polaron and bipolaron species as shown for IDTBT-P50 (28 nm) in Figure 5d). The bi-exponential dynamics show a fast decay of the neutral species together with a fast rise of polarons and slightly slower rise of bipolarons at a doping voltage of -0.9 V. The conversion speeds up with higher voltage because the driving force increases at a higher overpotential with respect to the doping onset (Figure S19). To compare the different materials, two voltages were chosen for each (-1.0 and -1.3 V for IDTBT-P0 and P10, -0.9

and -1.2 V for IDTBT-P50 and -0.8 and -1.1 V for IDTBT-P100), taking into account the different oxidation onsets. As the ion transport is hypothesized to be better for the more polar polymers, the kinetics is expected to vary for the IDTBT-P0 to P100 materials. This effect will also be impacted by the film thickness, since in our device configuration, the ions must penetrate vertically through the film to compensate the holes injected at the underlying ITO electrode. We hypothesise that ions penetrate through thinner films faster, until a limit is reached where the electrochemical reaction is slower than the ion penetration and the kinetics depend less on film thickness (Figure S20). Single-wavelength dynamics were used to display the dependence of the oxidation reaction rate on the applied voltage and the thickness (Figure S21, Table S3). Dynamics for 5-6 thicknesses ranging from around 8 to 200 nm for each IDTBT polymer were analysed, so that a clear sub-linear relation between doping/dedoping rate with the thickness can be observed. The precise thickness-dependent transport will be subject to a further study. For moving-front experiments over micrometre lateral film distances, it has been shown to occur by complex drift-diffusion mechanisms that include the applied potential and quasi-electric fields generated by charges in the film.[28]

For the present study, we simply compare thinner films of ~25 nm (close to the electrochemical limit) to thicker films of ~200 nm (strong dependence on ionic transport) for the different polymers. All doping and dedoping dynamics are shown in Figures S22 and S23. The data were analysed by MCR, and the kinetics were quantified by the time to reach 1/e of the final population (interpolating between two points close to 1/e) and are summarized in Table 1 and Table S4. In Figure 5e the temporal evolution of the neutral species is compared between the different IDTBT polymers for the two film thicknesses at the lower (-0.8 to -1.0 V) doping level. In the thinner films, IDTBT-P0 dopes the slowest with a time of 0.682 s to deplete 1/e of the neutral population, followed by IDTBT-P10 (0.336 s). This time decreases by more than half for the polar IDTBT-P50 and IDTBT-P100 polymers (0.138-0.187 s), which have very similar dynamics. Those polar polymers are close to the electrochemical limit, and the dynamics mainly correspond to the charge injection into the IDTBT backbone at a given overpotential (Figure S20). For the less polar derivatives with

less favourable ionic transport, thinner films (~8 nm) are necessary to reach the electrochemical limit, so that the dynamics in the ~25 nm films are still limited by ion transport and therefore slower. The same trend is seen for the 1/e rise of the polarons and bipolarons, which slows down from 0.145 s to 0.624 s (polarons) and from 0.309 s to 0.759 s (bipolarons) with decreasing polarity (Figure S22). In the thicker films, the doping process is overall slower by a factor of 1.5-2 compared to the thin films (Figure S22, Table 1), because of the higher impact of ionic transport. The effect is enhanced for the non-polar films, so that the difference between the materials becomes accentuated (Figure 5e). At the higher doping level (-1.1 to -1.3 V), all the doping dynamics are faster, and a similar increase of doping rate with polar side chain content is seen, especially for the thicker films (Figure S23). The dynamics were also investigated for the dedoping processes. A faster kinetic behaviour is observed during the dedoping of all polymers compared to the doping. However, the polar polymers again respond significantly faster than IDTBT-P0 even in the thin films (Figure 5f), showing that poor ionic transport also limits the dedoping rate. These results extracted from the dynamics of the MCR agree with the findings from the single-wavelength dynamics (Figures S21) and are very reproducible (Figure S24, Table S5).

Table 1: Time to reach 1/e of the formation respectively decay of the species at lower doping levels of -0.8 to -1.0 V (N = neutral; P = polaron; B = bipolaron). The errors represent the scatter of the curves. The total experimental error amounts to about ± 0.04 s.

Polymer	**N (s)**		**P (s)**		**B (s)**	
	thin	**thick**	**thin**	**thick**	**thin**	**thick**
IDTBT-P0	0.68 ± 0.02	0.96 ± 0.00	0.62 ± 0.03	0.84 ± 0.01	0.76 ± 0.01	1.37 ± 0.00
IDTBT-P10	0.34 ± 0.01	0.65 ± 0.02	0.20 ± 0.01	0.41 ± 0.03	0.51 ± 0.00	1.07 ± 0.01
IDTBT-P50	0.14 ± 0.01	0.33 ± 0.01	0.08 ± 0.02	0.16 ± 0.03	0.26 ± 0.00	0.69 ± 0.12
IDTBT-P100	0.19 ± 0.01	0.24 ± 0.01	0.15 ± 0.01	0.15 ± 0.02	0.31 ± 0.00	0.32 ± 0.01

Electronic transport and chemical doping

Having confirmed, both experimentally and computationally, that the IDTBT derivatives with polar side chain motifs indeed do facilitate ion movement in and out of the bulk polymer film, we next investigated the electronic transport properties of the system. As mentioned above, the charge transport of IDTBT is governed by fast intrachain transport and a limited number of close interchain contacts that allow for charge hopping across polymer chains. With this in mind, we first investigated *in silico* the effect of polar side chains and water and ion uptake on the number and quality of interchain contacts in IDTBT.

The analysis of the spatial contacts between polymer chains in the simulated morphologies of pure IDTBT-P0 and IDTBT-P100 without water or ions, as quantified in Figure S12 and Table 2, suggests a larger number of connecting pathways for charge hopping in IDTBT-P100 compared to IDTBT-P0. This result is corroborated by the calculated distribution of hole couplings.[29,30] Our density functional theory (DFT) calculations indeed reveal that, among all close contacts, the fraction that yields transfer integrals in excess of 1 meV is 37% in IDTBT-P100, compared to only 31% in IDTBT-P0 (Table 2). The difference is even more pronounced for strongly electronically coupled chromophores (transfer integrals in excess of 10 meV), which amount to 9% in IDTBT-P100 compared to 5% in IDTBT-P0. Based on the analysis of the density and quality of the close contacts between the polymer chains, substituting the apolar side chains of the original IDTBT copolymer by more flexible polar side chains is thus not expected to alter the outstanding charge transport properties of the original IDTBT copolymer, quite the opposite. Moving on from the pure polymer films, we consider next the swollen systems more relevant for OECT device operation. In the case of IDTBT-P100 subjected to 5% and 25% water uptake, we find that the higher the water intake the smaller the density of intermolecular electronic contacts, though the effect is rather modest (except for the most strongly interacting pairs), see Table 2. This decrease in electronic connectivity is driven by the swelling of the polymer film in the presence of water. Furthermore, the simultaneous presence of water and anions in the film does not alter the connectivity between the monomeric units (Table 2,

last entry). Although the total number of contacts is slightly reduced compared to pure IDTBT-P100 films (111 versus 124), the quality of the strongest electronic contacts is similar to what was found for pure P100 (11% versus 9% of contacts with hole couplings larger than 10 meV). This suggests that, from an electronic connectivity point of view, the intrinsic charge transport properties of pure IDTBT-P100 should be preserved in OECT devices.

Table 2: Number and quality of close interchain contacts in IDTBT-P0 and IDTBT-P100.

Polymer	Water content	Close contacts	Contacts w. t_{HOMO} > 10 meV	Contacts w. t_{HOMO} > 5 meV	Contacts w. t_{HOMO} > 1 meV
IDTBT-P0	0%	93	5%	12%	31%
IDTBT-P100	0%	124	9%	14%	37%
IDTBT-P100	5%	110	7%	16%	35%
IDTBT-P100	25%	100	5%	17%	40%
IDTBT-P100[a]	25%	111	11%	19%	42%

All systems comprise 20 hexamers; [a] System doped with 60 positive charges and 60 Cl^- counter ions. t_{HOMO} denotes the highest occupied molecular orbital (HOMO) electronic transfer coupling.

In contrast to the encouraging computational results on the electronic properties of the polar IDTBT derivatives, experimental data suggests otherwise. First, we fabricated organic field-effect transistors (OFETs) to evaluate the charge carrier mobilities across the IDTBT series (Figures S25-S26 and Table 3). A saturation hole mobility of 0.95 cm^2/Vs was found for IDTBT-P0 in good agreement with previous studies.[18] Nevertheless, introduction of polar side chains afforded a rapid decline in the transport properties with the hole mobility decreasing steeply to 0.34 cm^2/Vs and $7.8 \cdot 10^{-3}$ cm^2/Vs for IDTBT-P10 and IDTBT-P50, respectively, while no current modulation could be observed for the IDTBT-P100 device. Such trends have been observed previously for other p- and n-type semiconducting polymers.[22,31] To investigate if residual water in the more polar IDTBT films

played a role in the poor device performance, we also fabricated OFETs with a molecular additive (2,3,5,6-tetrafluoro-7,7,8,8-tetracyanoquinodimethane, F4TCNQ).[32,33] No improvement in device performance was observed with the F4TCNQ additive (Figure S27) indicating that residual water is not responsible for the decline in charge carrier mobility with increasing polar content or that the adverse effect of residual water cannot be avoided by the incorporation of molecular additives as it can for the IDTBT-P0 polymer.

Subsequently, IDTBT films spin-cast onto glass substrates were chemically doped using the strong oxidant tris(4-bromophenyl)ammoniumyl hexachloroantimonate (Magic Blue) to investigate their electrical conductivity using four-point probe measurements. The polymers were doped sequentially using two different dopant concentrations, 0.25 mg/mL and 0.5 mg/mL of Magic Blue in acetonitrile, to achieve different doping levels (Figure S28). Again, a rapid decline in electrical performance was observed with increasing polar content (Table 3). At low doping levels, a more than 100-fold decrease in conductivity was seen when going from IDTBT-P0 to IDTBT-P50 in line with the OFET data. The conductivity is generally higher at the higher doping level (0.5 mg/mL) with the trend of decreasing conductivity with increasing polar content similar, although the drop in conductivity is smaller (4.49 S/cm versus 0.93 S/cm for IDTBT-P0 and IDTBT-P50, respectively). For both doping levels, no current could be detected for IDTBT-P100 with the used technique in good agreement with the transistor data. Although the relatively low molecular weight of IDTBT-P100 could be a contributing factor to the low OFET mobility and the low conductivity upon doping, the three other IDTBT derivatives are of comparable molecular weight confirming that the observed charge transport trends are unlikely to be dominated by molecular weight effects.

Table 3: Field-effect transistor characteristics of the IDTBT polymers and electrical conductivity of the IDTBT polymers at different chemical doping levels.

Polymer	μ_{sat} (cm^2/Vs)[a]	V_{th}^{sat} (V) (reverse/forward)	I_{on}/I_{off}	Conductivity (S/cm)[b]	Conductivity (S/cm)[c]
IDTBT-P0	0.95	-26.4/-26.4	$4.87 \cdot 10^5$	1.06	4.49
IDTBT-P10	0.34	-19.4/-18.2	$4.80 \cdot 10^4$	$2.77 \cdot 10^{-2}$	2.65
IDTBT-P50	$7.8 \cdot 10^{-3}$	-18.9/-5.89	65.7	$8.64 \cdot 10^{-3}$	$9.26 \cdot 10^{-1}$
IDTBT-P100	/	/	/	/	/

[a] The saturation hole mobility (μ_{sat}) is a maximum value extracted at a drain voltage of -60 V; [b] doped with Magic Blue (0.25 mg/ml); [c] doped with Magic Blue (0.50 mg/ml).

With the computational modelling suggesting little or no negative effect on the number and quality of interchain contacts upon the introduction of polar side chains onto IDTBT, increasing energetic disorder was considered as an alternative explanation for the deterioration of charge transport properties that we observe experimentally with increasing polar side chain content.[34] In order to test this hypothesis, we theoretically assessed the electrostatic energetic disorder in IDTBT-P100 (both dry and wet) versus IDTBT-P0, in both amorphous and crystalline morphologies of the polymers. As a proxy for the energetic disorder, we computed the standard deviation on the total energy of the films when adding one excess positive charge on successively each single monomer unit of each polymer chain. Table 4 shows that, in their respective amorphous phases, the standard deviation calculated in dry IDTBT-P100 is about three times as large as that in IDTBT-P0 (113 meV versus 43 meV). Interestingly, the presence of water in amorphous IDTBT-P100 does not lead to a further increase of the energetic disorder. Since IDTBT-P0 and IDTBT-P100 both exhibit a near-amorphous character and conformational disorder resilient energetic disorder, the main culprit for the increased energetic inhomogeneity in IDTBT-P100 is the varying electrostatic potential induced on the conjugated backbones by the polar side chains, as indeed confirmed by a detailed analysis of the various contributions to the total potential energy. In hypothetical crystalline morphologies, we expect the electrostatic potential to be more homogeneous and hence the energetic disorder to be

smaller. This is, indeed, what is predicted by the calculations, see Table 4. We note, however, that even in the crystalline phase, where the side chains are kept away from their conjugated cores due to the interdigitated lamellar organisation, there is a residual energetic inhomogeneity with a similar trend of increased energetic disorder in the polar system. This is because of the combined effects of thermal motion and the fact that holes sitting on one lamellar layer still feel the electrostatic effects associated with side chains belonging to the adjacent lamella (see Figure S8). As a matter of fact, the distance between the last carbon of the side chains and the closest conjugated atom of the next lamellar layer is only ~2.5Å.

Table 4: DFT-calculated standard deviation of the energetic disorder when adding one excess positive charge successively on each monomer of each IDTBT-P0 and IDTBT-P100 polymer chain.

Polymer	**Morphology**	**Standard deviation (meV)**
IDTBT-P0	Amorphous	43
IDTBT-P100	Amorphous	113
IDTBT-P100	Amorphous (5% water)	109
IDTBT-P100	Amorphous (25% water)	110
IDTBT-P0	Crystalline	22
IDTBT-P100	Crystalline	46

All systems comprise 20 hexamers.

Photothermal deflection spectroscopy was subsequently performed on the polymer series to investigate experimentally the energetic disorder in the system (Figure S29). Urbach energy values of 29.8 meV, 30.8 meV, 32.0 meV, and 43 meV for IDTBT-P0, P10, P50 and P100, respectively, confirmed the increasing energetic disorder with increasing polar content; a significantly higher energetic disorder for IDTBT-P100 is in qualitative agreement with the predictions from the

computational modelling. We note that the lower molecular weight and higher polydispersity of IDTBT-P100 could also contribute to the higher Urbach energy.

Conclusion and outlook

Indacenodithiophene-*co*-benzothiadiazole, a high-performing electronic charge transport material, was synthetically modified with amphipathic side chains comprising an apolar five-methylene spacer and a polar terminal oligoether group to impart mixed ionic-electronic transport properties. A series of polymers was prepared with varying polar content and studied extensively using a suite of experimental and computational techniques. Expectedly, we saw increasing water uptake and faster ion kinetics in the polymer films with increasing polar content. This was firmly established using time-resolved spectroelectrochemistry on both relatively thin and thick polymer films. Despite the successful chemical engineering of ion-transport pathways in the polymer films with higher polar content, mixed ionic-electronic properties probed in an organic electrochemical transistor configuration were lacking with negligible electrical current modulation observed for the polar IDTBT polymers. The underlying lack of efficient electronic charge transport in the polar polymer derivatives was ultimately found to originate not from a deterioration of intrachain contacts but from an increasing energetic inhomogeneity caused by the oligoether segments of the side chains.

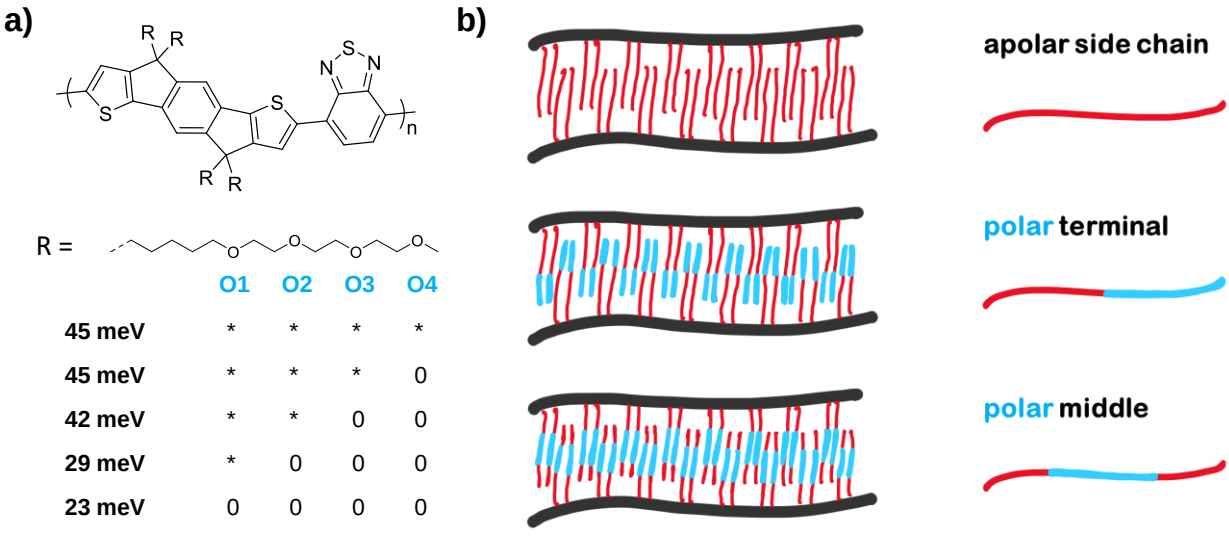

	O1	O2	O3	O4
45 meV	*	*	*	*
45 meV	*	*	*	0
42 meV	*	*	0	0
29 meV	*	0	0	0
23 meV	0	0	0	0

Figure 6*: (a) DFT-calculated standard deviation of the energetic disorder in IDTBT-P100 (cofacial stacking) when tuning the atomic charges along the oligoether segment of the side chain. The values are obtained from the analysis of the last frame of the 1 ns MD (NPT, p = 1 atm, T = room temperature). The atomic charges are estimated at the electrostatic potential quantum-chemical level (*) and set to 0 for zero atomic charges where indicated; (b) schematic illustration of cofacial polymer packing with side chain interdigitation giving rise to close proximity between the polar terminus (middle image) of a side chain and the neighbouring polymer backbone; this distance could be increased if the polar segment is moved to the middle of the side chain (bottom image).*

To better gauge the origin of the observed electrostatic disorder in the polar IDTBT systems, we have performed Gedanken numerical experiments where the partial atomic charges of the oxygen atoms in the oligoether moiety have been set to zero one after the other (Figure 6a) while freezing all nuclei. We find, in particular, that the amount of energetic disorder is significantly reduced when the partial charges over the last two oxygen atoms (O3 and O4 in Figure 6a) are set to zero as for apolar groups. Overall, our results suggest that the poor performance of IDTBT-P100 in OECTs is likely because of the poorly organised character of the film and the associated additional source of disorder introduced by the polar side chains. Increasing the degree of structural order in the polymer films thus appears as an attractive strategy, especially if it can be combined with the use of mixed (amphipathic) side chains for water and ion intake where the polar moieties are properly placed near the middle to maximize their separation from the conjugated backbones from the same or adjacent layers (Figure 6b).

Considering why IDTBT behaves differently to other semiconducting polymers that have been structurally modified to impart mixed ionic-electronic transport properties we believe it is related to the microstructure and the mechanism of charge transport. Because IDTBT has no pronounced, close π-π stacking the electronic charge transport is particularly sensitive to the presence of energetic disorder in the vicinity of the sites at which interchain hopping occurs. The presence of

polar side chains, which are introduced in a random fashion along the polymer chain due to the statistical polymerisation process and have permanent dipoles and a different conformation compared to linear alkyl chains, in the vicinity of the close interchain contacts can introduce energetic barriers for the interchain hopping process that the electronic charge carrier mobility is very sensitive to.

In conclusion, when considering the learning outcomes from this study in the context of future molecular design strategies, our experimental work and combined classical/quantum simulations have shown that the performance of OECT devices can be strongly altered by the presence of polar side chains. Their interactions with the conjugated backbone can lead to a dramatic increase of the energetic disorder. However, two strategies can limit this increase: (i) the use of semi-crystalline instead of near-amorphous organic semiconductors and (ii) the judicious design of the polar side chains, *i.e.*, by incorporating the hydrophilic segment between two apolar regions.

Author Contributions

I.H.: investigation, formal analysis, writing; V.L.: investigation, formal analysis, writing; M.W.: investigation, formal analysis, writing; H.-Y.W.: investigation, formal analysis, writing; L.Z.: investigation, formal analysis; R.M.-H.: formal analysis, writing; P.G.-F.: investigation, formal analysis; P.C.: investigation, formal analysis; S.H.: investigation, formal analysis; D.M.: investigation, formal analysis; R.W.: investigation, formal analysis; B.D.P.: formal analysis; J.S.: investigation; A.L.: investigation, formal analysis; J.R.: supervision; H.S.: supervision; N.B.: conceptualization, supervision, writing; D.B.: conceptualization, supervision, writing; S.F.: conceptualization, supervision, writing; C.B.N.: conceptualization, supervision, writing.

Acknowledgements

We acknowledge funding from the European Commission Horizon 2020 Future and Emerging Technologies (FET) project MITICS (964677). The computational resources in Mons are supported by the FNRS "Consortium des Equipements de Calcul Intensif−CECI" program Grant No. 2.5020.11 and by the Walloon Region (ZENOBE Tier-1 supercomputer, under grant 1117545). R.W. and J.R. acknowledge support from the National Science Foundation, NSF award DMR-1751308. This research used resources of the Advanced Photon Source; a U.S. Department of Energy (DOE) Office of Science User Facility operated for the DOE Office of Science by Argonne National Laboratory under Contract No. DE-AC02-06CH11357. D.B. is FNRS Research Director.

References

1 B. D. Paulsen, K. Tybrandt, E. Stavrinidou and J. Rivnay, *Nat. Mater.*, 2020, **19**, 13–26.

2 F. Torricelli, D. Z. Adrahtas, Z. Bao, M. Berggren, F. Biscarini, A. Bonfiglio, C. A. Bortolotti, C. D. Frisbie, E. Macchia, G. G. Malliaras, I. McCulloch, M. Moser, T.-Q. Nguyen, R. M. Owens, A. Salleo, A. Spanu and L. Torsi, *Nat. Rev. Methods Prim.*, 2021, **1**, 66.

3 C. J. Kousseff, R. Halaksa, Z. S. Parr and C. B. Nielsen, *Chem. Rev.*, 2022, **122**, 4397–4419.

4 J. Rivnay, P. Leleux, M. Ferro, M. Sessolo, A. Williamson, D. A. Koutsouras, D. Khodagholy, M. Ramuz, X. Strakosas, R. M. Owens, C. Benar, J.-M. J. M. Badier, C. Bernard and G. G. Malliaras, *Sci. Adv.*, 2015, **1**, e1400251.

5 M. J. Donahue, A. Sanchez-Sanchez, S. Inal, J. Qu, R. M. Owens, D. Mecerreyes, G. G. Malliaras and D. C. Martin, *Mater. Sci. Eng. R Reports*, 2020, **140**, 100546.

6 Y. Kim, H. Noh, B. D. Paulsen, J. Kim, I. Y. Jo, H. J. Ahn, J. Rivnay and M. H. Yoon, *Adv. Mater.*, 2021, **33**, 2007550.

7 A. Giovannitti, D.-T. Sbircea, S. Inal, C. B. Nielsen, E. Bandiello, D. A. Hanifi, M. Sessolo, G. G. Malliaras, I. McCulloch and J. Rivnay, *Proc. Natl. Acad. Sci.*, 2016, **113**, 12017–12022.

8 T. Nicolini, J. Surgailis, A. Savva, A. D. Scaccabarozzi, R. Nakar, D. Thuau, G. Wantz, L. J. Richter, O. Dautel, G. Hadziioannou and N. Stingelin, *Adv. Mater.*, 2020, **33**, 2005723.

9 A. T. Lill, D. X. Cao, M. Schrock, J. Vollbrecht, J. Huang, T. Nguyen-Dang, V. V. Brus, B. Yurash, D. Leifert, G. C. Bazan and T. Q. Nguyen, *Adv. Mater.*, 2020, **32**, 1908120.

10 Z. S. Parr, R. B. Rashid, B. D. Paulsen, B. Poggi, E. Tan, M. Freeley, M. Palma, I. Abrahams, J. Rivnay and C. B. Nielsen, *Adv. Electron. Mater.*, 2020, **6**, 2000215.

11 C. B. Nielsen, A. Giovannitti, D.-T. T. Sbircea, E. Bandiello, M. R. Niazi, D. A. Hanifi, M. Sessolo, A. Amassian, G. G. Malliaras, J. Rivnay and I. Mcculloch, *J. Am. Chem. Soc.*, 2016, **138**, 10252–10259.

12 A. Giovannitti, C. B. Nielsen, D.-T. T. Sbircea, S. Inal, M. Donahue, M. R. Niazi, D. A. Hanifi, A. Amassian, G. G. Malliaras, J. Rivnay and I. Mcculloch, *Nat. Commun.*, 2016, **7**, 13066.

13 M. Moser, A. Savva, K. Thorley, B. D. Paulsen, T. C. Hidalgo, D. Ohayon, H. Chen, A. Giovannitti, A. Marks, N. Gasparini, A. Wadsworth, J. Rivnay, S. Inal and I. McCulloch, *Angew. Chemie*, 2021, **133**, 7856–7864.

14 G. Krauss, F. Meichsner, A. Hochgesang, J. Mohanraj, S. Salehi, P. Schmode and M. Thelakkat, *Adv. Funct. Mater.*, 2021, **31**, 2010048.

15 E. Tan, J. Kim, K. Stewart, C. Pitsalidis, S. Kwon, N. Siemons, J. Kim, Y. Jiang, J. M. Frost, D. Pearce, J. E. Tyrrell, J. Nelson, R. M. Owens, Y. H. Kim and J. S. Kim, *Adv. Mater.*, 2022, **34**, 2202574.

16 Y. Wang, E. Zeglio, H. Liao, J. Xu, F. Liu, Z. Li, I. P. Maria, D. Mawad, A. Herland, I. Mcculloch and W. Yue, *Chem. Mater.*, 2019, **31**, 9797–9806.

17 Z. S. Parr, J. Borges-González, R. B. Rashid, K. J. Thorley, D. Meli, B. D. Paulsen, J. Strzalka, J. Rivnay and C. B. Nielsen, *Adv. Mater.*, 2022, **34**, 2107829.

18 W. Zhang, J. Smith, S. E. Watkins, R. Gysel, M. McGehee, A. Salleo, J. Kirkpatrick, R. S. Ashraf, T. D. Anthopoulos, M. Heeney and I. McCulloch, *J. Am. Chem. Soc.*, 2010, **132**, 11437–11439.

19 X. Zhang, H. Bronstein, A. J. Kronemeijer, J. Smith, Y. Kim, R. J. Kline, L. J. Richter, T. D. Anthopoulos, H. Sirringhaus, K. Song, M. Heeney, W. Zhang, I. McCulloch and D. M. Delongchamp, *Nat. Commun.*, 2013, **4**, 2238.

20 I. Dobryden, V. V. Korolkov, V. Lemaur, M. Waldrip, H.-I. Un, D. Simatos, L. J. Spalek, O. D. Jurchescu, Y. Olivier, P. M. Claesson and D. Venkateshvaran, *Nat. Commun.*, 2022, **13**, 3076.

21 D. Venkateshvaran, M. Nikolka, A. Sadhanala, V. Lemaur, M. Zelazny, M. Kepa, M. Hurhangee, A. J. Kronemeijer, V. Pecunia, I. Nasrallah, I. Romanov, K. Broch, I. McCulloch, D. Emin, Y. Olivier, J. Cornil, D. Beljonne and H. Sirringhaus, *Nature*, 2014, **515**, 384–388.

22 P. A. Finn, I. E. Jacobs, J. Armitage, R. Wu, B. D. Paulsen, M. Freeley, M. Palma, J. Rivnay, H. Sirringhaus and C. B. Nielsen, *J. Mater. Chem. C*, 2020, **8**, 16216–16223.

23 A. Kahn, *Mater. Horizons*, 2016, **3**, 7–10.

24 O. Fenwick, C. Van Dyck, K. Murugavel, D. Cornil, F. Reinders, S. Haar, M. Mayor, J. Cornil and P. Samorì, *J. Mater. Chem. C*, 2015, **3**, 3007–3015.

25 V. Lemaur, J. Cornil, R. Lazzaroni, H. Sirringhaus, D. Beljonne and Y. Olivier, *Chem. Mater.*, 2019, **31**, 6889–6899.

26 I. E. Jacobs, G. D'avino, V. Lemaur, Y. Lin, Y. Huang, C. Chen, T. F. Harrelson, W. Wood, L. J. Spalek, T. Mustafa, C. A. O'keefe, X. Ren, D. Simatos, D. Tjhe, M. Statz, J. W. Strzalka, J. K. Lee, I. Mcculloch, S. Fratini, D. Beljonne and H. Sirringhaus, *J. Am. Chem. Soc.*, 2022, **144**, 3005–3019.

27 S. H. Kim, H. Yook, W. Sung, J. Choi, H. Lim, S. Chung, J. W. Han and K. Cho, *Adv. Mater.*, 2023, **35**, 2207320.

28 S. T. Keene, A. Rao and G. G. Malliaras, *Sci. Adv.*, 2023, **9**, eadi3536.

29 T. H. Thomas, D. J. Harkin, A. J. Gillett, V. Lemaur, M. Nikolka, A. Sadhanala, J. M. Richter, J. Armitage, H. Chen, I. McCulloch, S. M. Menke, Y. Olivier, D. Beljonne and H. Sirringhaus, *Nat. Commun.*, 2019, **10**, 2614.

30 R. Dilmurat, V. Lemaur, Y. Olivier, S. M. Gali and D. Beljonne, *J. Phys. Chem. C*, 2022, **126**, 3118–3126.

31 A. Giovannitti, I. P. Maria, D. Hanifi, M. J. Donahue, D. Bryant, K. J. Barth, B. E. Makdah, A. Savva, D. Moia, M. Zetek, P. R. F. Barnes, O. G. Reid, S. Inal, G. Rumbles, G. G. Malliaras, J. Nelson, J. Rivnay and I. McCulloch, *Chem. Mater.*, 2018, **30**, 2945–2953.

32 M. Nikolka, I. Nasrallah, B. Rose, M. K. Ravva, K. Broch, A. Sadhanala, D. Harkin, J. Charmet, M. Hurhangee, A. Brown, S. Illig, P. Too, J. Jongman, I. McCulloch, J.-L. L. Bredas and H. Sirringhaus, *Nat. Mater.*, 2017, **16**, 356–362.

33 M. Nikolka, G. Schweicher, J. Armitage, I. Nasrallah, C. Jellett, Z. Guo, M. Hurhangee, A. Sadhanala, I. McCulloch, C. B. Nielsen and H. Sirringhaus, *Adv. Mater.*, 2018, **30**, 1801874.

34 B. Xu, X. Yi, T. Y. Huang, Z. Zheng, J. Zhang, A. Salehi, V. Coropceanu, C. H. Y. Ho, S. R.

Marder, M. F. Toney, J. L. Brédas, F. So and J. R. Reynolds, *Adv. Funct. Mater.*, 2018, **28**, 1803418.